Robotica (2010) volume 28, pp. 149–159. © Cambridge University Press 2009
doi:10.1017/S0263574709005670

Blend of independent joint control and variable structure systems for uni-drive modular robots

Hamidreza Karbasi, Jan Paul Huissoon* and Amir Khajepour

Department of Mechanical and Mechatronics Engineering, University of Waterloo, Waterloo, Ontario, Canada N2L 3G1

(Received in Final Form: April 8, 2009. First published online: May 22, 2009)

SUMMARY

In this paper, a control design methodology for a new class of modular robots, so-called "uni-drive modular robots" is introduced. Uni-drive modular robots have a substantial advantage over regular modular robots in terms of the mass of each module since then employ only a single drive for powering all the joints. The drive is mounted at the robot base and all joints tap power from this single drive using clutches. By controlling the engagement time of the clutches, the position and velocity of the joints are regulated. After reviewing the structure of the uni-drive modular robot, a self-expansion formula to generate the dynamics of the robot is introduced. The control of uni-drive n-module robots is realized by blending independent joint control and theory of variable structure systems via a pulse width modulation technique. A uni-drive modular robot is used to conduct simulations and validate the control design technique.

KEYWORDS: Modular robot; spring wrap clutch; sliding mode control.

1. Introduction

The concept of modularity has been proposed for the design of robot mechanisms to provide flexibility, economy, ease of maintenance, and rapid deployment.[1–9] A fully modular reconfigurable robot consisting of a set of standardized modules can be configured to different structures and degrees of freedom (DOFs) for different task requirements. The feasibility of the modular approach has been carried out using various prototypes built at several research institutes.[1,6,7,9–11] Modules may have different output powers to provide a wide variety of configurations;[6,9,12] however, the common feature of all current modular robots is the use of self-actuated modules. A good overview of the topic and challenges and opportunities can be found in ref. [13].

One example of a modular robot is Polypod.[14] This modular robot is constructed using two different modules. The first module is called a segment with 2 DOFs, and the second module is called a node to supply power to the segments. In ref. [14], the author demonstrated the capability of the Polypod by constructing different configurations such as a caterpillar, an earthworm, and a slinky using these two modules.

Although the modular design philosophy has several advantages, the mass of each module limits the number of units that can be chained together. In refs. [15, 16], a new modular robot concept, the so-called "uni-drive" modular robot has been introduced to remove this limitation. In ref. [17], extensive design, modeling, and simulation studies have been reported for uni-drive modular robots. An experimental two-axis gantry robot based on this concept was designed and fabricated. The mathematical model of the gantry robot was developed and simulation results were compared. In a uni-drive modular robot, one drive motor mounted at the base is used to power all the modules through a rotating shaft and clutches. The engagement of the clutches is controlled by the pulse width modulation (PWM) technique to regulate velocity and position of the modules.

In ref. [18], a mechanism with a single-motor actuation is introduced for a dexterous hand. In this mechanism, seven bilateral clutches were used to actuate three fingers.

The discontinuous PWM controller design of a robotic manipulator has been reported in ref. [19]. In this work, the discontinuous (on-off) stabilizing controller was determined from a continuous controller designed for the nonlinear average model of the PWM controlled system. The combination of a sliding mode controller with PWM has also been reported for controlling an antilock brake system (ABS) and position control of an x–y table mechanism.[20,21]

In following sections, the concept and overall structure of the uni-drive modular robot are first explained. The design of the mechanical drive using a spring wrap clutch (SWC) used to regulate the output speed of the mechanical drive is also reviewed. A self-expansion formula is introduced as a suitable tool for modeling of modular robots. Finally, simulation results to assess the robustness of the designed controller are presented.

2. Uni-drive Modular Robots

In Figs. 1 and 2, two different configurations of uni-drive modular robots are depicted. In Fig. 1, the modules are in series while in Fig. 2 they are in parallel. In both configurations, the robot consists of n modules, each taking their power from a common drive shaft. In the series design, a single drive at the base powers all the joints through a central rotating shaft and mechanical drive units. These units are designed to use a unidirectional input to provide a bidirectional output using two SWCs although alternative clutch designs are also clearly feasible. The PWM technique is used to control the clutches, and as a result, the average output velocity of the units can be varied within a desired

*Corresponding author. E-mail: jph@mecheng1.uwaterloo.ca

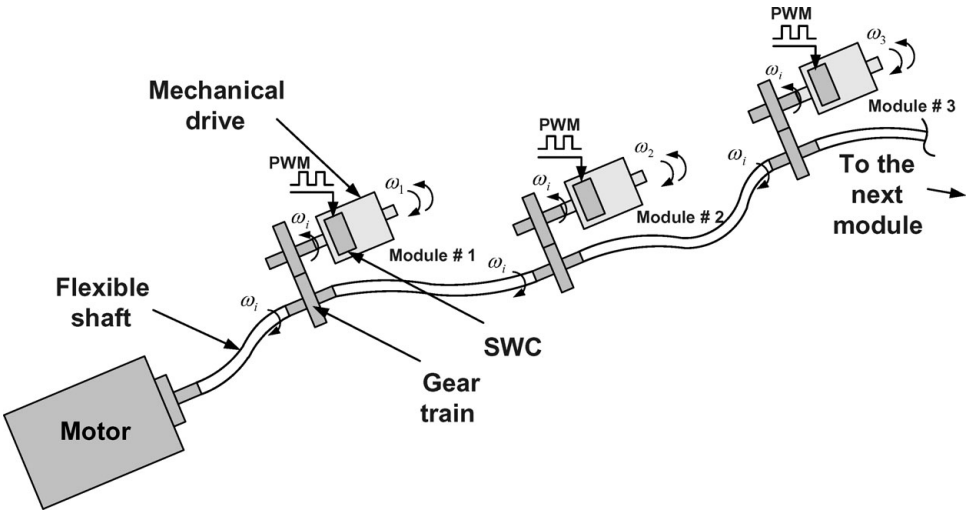

Fig. 1. Series configuration of the uni-drive modular robot.

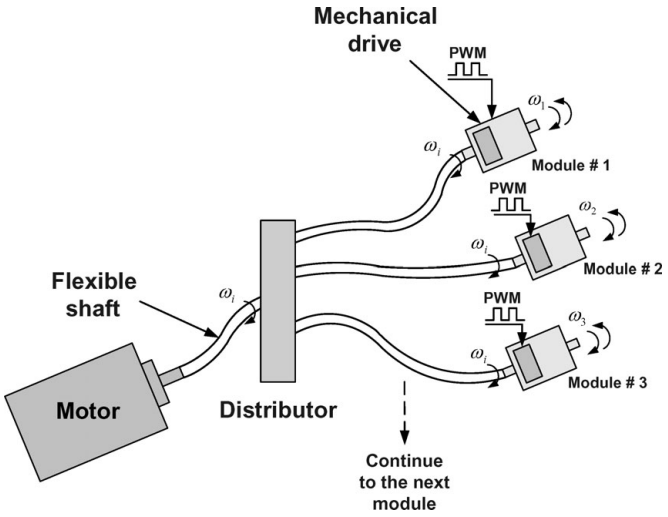

Fig. 2. Parallel configuration of the uni-drive modular robot.

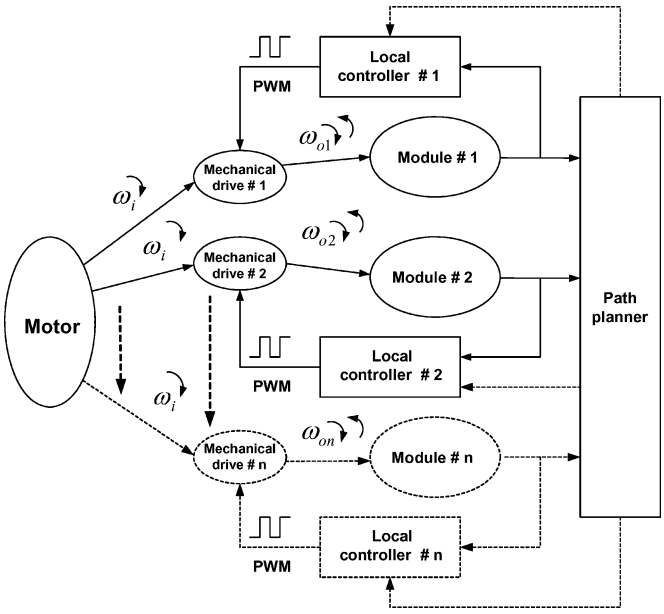

Fig. 3. Schematic of the uni-drive modular robot control system.

range. In the parallel design, each mechanical drive is connected to a distributor via a rotating shaft powered by the single drive.

This new class of robots has several advantages over conventional modular robot designs in which the actuators are placed at, or close to, the joints. These advantages include: lower manufacturing cost by reducing the complexity of actuators and controllers, higher dexterity and manipulability by chaining a larger number of modules together, and simplicity in drives and their control system by replacing continuous drives with clutches and on/off controllers.

The proposed modular robot can be used in inspection and repair of welds on tube bundles in nuclear heat exchangers (limited access and hazardous environment), working in a cluttered environment in which a dexterous and more flexible robot is needed, space applications where inertia is a major concern, and agile manufacturing where production requirements and configurations change frequently.

In Fig. 3, a proposed control scheme for the robot shown in Fig. 1 is presented. As shown in this figure, a motor mounted at the base feeds all mechanical drives with constant speed. The modules are powered and controlled by the mechanical drives using local controllers. The inputs and output of a local controller are the position and velocity of its module, and a tuned PWM signal, respectively. While the local controllers are used to control each module, a path planner is needed to supervise local controllers to accomplish the robot's main task and also to deal with redundancy in the robot.

2.1. Mechanical drive unit: design and modeling

To implement the conceptual design shown in Fig. 1, a mechanical drive is needed to differentiate the unidirectional speed of the central rotating shaft into forward and reverse motions. For this purpose, the mechanical drive unit shown in Fig. 4 is proposed. The unit consists of two SWCs (upper and lower), and spur and planetary gear trains. The planetary gear train has two inputs: the first is the pinion (sun), which is connected directly to the input shaft, and the second is the carrier. The carrier either can be locked to the frame by engaging the lower clutch, or can be driven from the input shaft via the spur gear train (gears 1 through 4) by engaging

https://doi.org/10.1017/S0263574709005670 Published online by Cambridge University Press

Table I. Four possible states for the mechanical drive.

Lower clutch	Upper clutch	State	Output
0	0	0	Free
0	1	1	Forward
1	0	2	Reverse
1	1	Disallowed	–

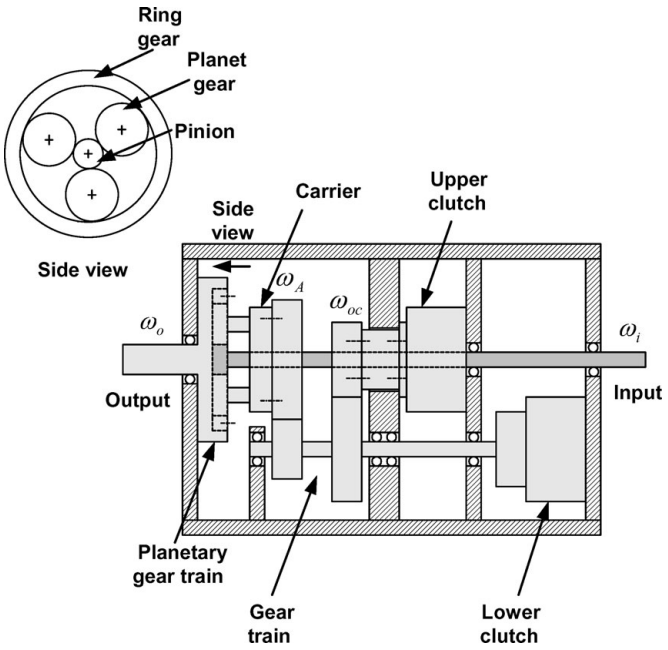

Fig. 4. Schematic of the mechanical drive.

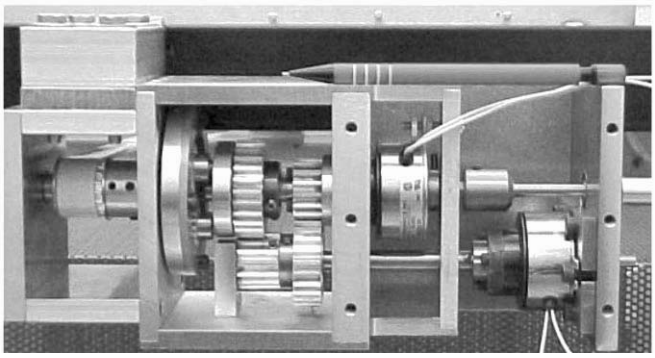

Fig. 5. Mechanical drive unit.

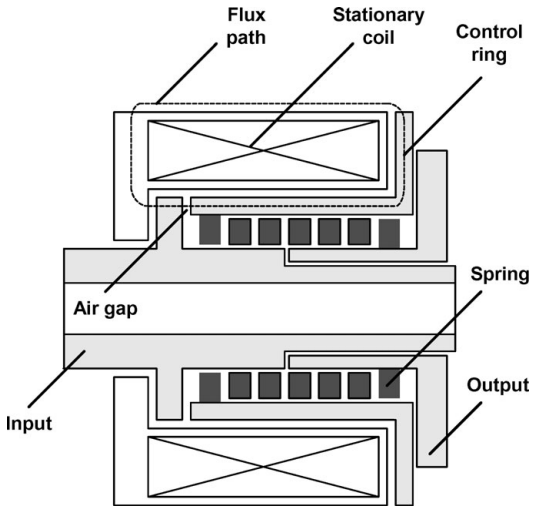

Fig. 6. Typical cross-section of a SWC.

the upper clutch. Three planet gears are mounted on the carrier and mesh with the pinion and ring gear as shown in Fig. 4. The ring gear drives the output shaft. There are four possible states for this two-clutch system as shown in Table I.

A prototype of the mechanical drive has been fabricated and is shown in Fig. 5. For this prototype, considering the number of gear teeth and the kinematics of the planetary gear train, the maximum forward and reverse speeds of the output shaft can be calculated as:[1]

$$\omega_{o\,(\text{forward})} = 0.2\omega_i \qquad \omega_{o\,(\text{reverse})} = -0.24\omega_i. \tag{1}$$

SWCs were selected for the mechanical drive due to their high power transmission to weight ratio and their rapid response time. A typical cross-section of an SWC is shown in Fig. 6. The key element of this clutch is the close coiled torsional spring, one end of which is attached to the output shaft and the other end to a control ring. A small air gap separates the end of the control ring from a collar on the input shaft when the clutch is disengaged. A stationary coil (solenoid) is used to engage the clutch by drawing the control ring against the collar on the input shaft. Friction between the control ring and input shaft causes the spring to wrap down, which makes the internal diameter of the spring smaller, and as a result mechanically connects the input shaft to the output. After the electric current is interrupted, the magnetic field is removed causing the spring to unwrap and thus disengage the clutch. This type of clutch relies on the relative rotation between the input and output shafts for engagement; thus the slower the input shaft speed the longer the engagement time. The wrap relative angle between the input and output shafts is typically 9°. SWCs also provide torque only in the direction in which they wrap down.

To model an SWC, the main elements including the magnetic circuit, the control ring motion and clutch function should be considered. A lumped model of an SWC is shown in Fig. 7. In this model, linear and rotational motions of the control ring are considered to be independent. For each motion, a mass-spring-damper mechanism is considered and the control ring is connected to the output by a torsional spring and to the ground by a linear spring. Its maximum linear and rotational motions are x_g and φ_g, respectively. For both independent linear and rotational movement of the control ring, absolute and relative viscous friction are considered.

Based on the above lumped model and certain other assumptions, the equations of motion become (for details see ref. [17]):

$$m\ddot{x} + b_l\dot{x} + k_l x = f_{sol}, \tag{2}$$

$$J\ddot{\varphi} + b_r(\dot{\varphi} - \dot{\theta}) + k_r(\varphi - \theta) + b_{ra}\dot{\varphi} = T_c, \tag{3}$$

$$J_{eff}\ddot{\theta} + b_r(\dot{\theta} - \dot{\varphi}) + k_r(\theta - \varphi) + b_{eff}\dot{\theta} = c(\omega_i - \dot{\theta}), \tag{4}$$

[1] For more details about this design the reader is referred to ref. [17].

https://doi.org/10.1017/S0263574709005670 Published online by Cambridge University Press

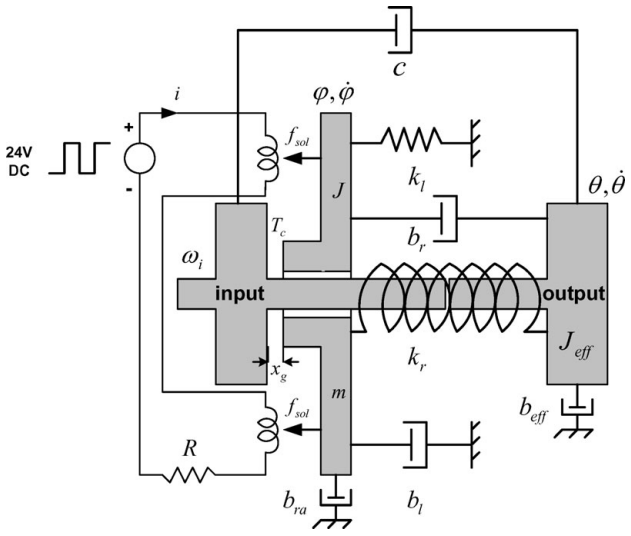

Fig. 7. Proposed lumped model for SWCs.

where m, J, J_{eff}, k_l, k_r, b_l, b_r, b_{ra}, and b_{eff} are the mass, moment of inertia, spring stiffness, and viscous friction coefficients shown in Fig. 7. Also f_{sol}, T_c, c, ω_i, θ, and φ are magnetic force, Coulomb torque, virtual[2] viscous coefficient, clutch input angular velocity, and angular displacement of clutch output and control ring, respectively. Equation (2) gives the forced linear motion of the control ring that is actuated by the magnetic force. Equation (3) represents the forced rotational motion of the control ring that is actuated by the Coulomb torque. Finally, Eq. (4) shows the forced rotational motion of the output that is actuated by virtual nonlinear viscous friction. In the overall model of the mechanical drive unit, J_{eff}, and b_{eff} represent the inertia and friction of the gear train. By modifying Eq. (4), the overall model of a uni-drive modular robot with any kind of modules (rotational/translational) can be derived.

In subsequent sections, the dynamics of an n-module planar robot will first be introduced. Integration of the mechanical drive into the robot dynamics will be developed next. The remainder of paper will deal with control of such robots using concepts of independent joint control, theory of variable structure (VS) systems, and PWM technique.

3. Uni-Drive n-Module Planar Robot

In this section, the concept of the uni-drive modular robot introduced in the previous section will be applied to a planar robot. For this purpose, a self-expansion formula (SEF) for planar modular robots is considered. Assuming unified modules, the SEF generates the equations of motion for the modular robot based upon the number of modules. The integration of the SEF and the developed model of the mechanical drive will yield the final dynamics of the uni-drive n-module planar robot in the form of an SEF.

[2] In a SWC as the torsional spring wraps down, the output torque increases linearly in a short period of time and the output velocity becomes equal to the input velocity rapidly. To model this, it is assumed a virtual viscous friction acting between the input and output shafts (for details see ref. [17]).

3.1. Self-Expansion Formula

For control design purposes, it is necessary to have a mathematical model that describes the dynamic behavior of the system. However, for a modular robot, it is very helpful to have an SEF. The SEF generates the whole set of robot dynamic equations based on only the number of modules. Here, our approach to derive such a formula relies on the Euler–Lagrange technique. In Fig. 8 the planar configuration of a modular robot is shown. All n modules are the same, and have 2 DOF each, one rotational and one translational. Therefore, the whole robot has $2n$ DOF.

Although the structure shown in Fig. 8 is planar, by considering the different rotational axes' directions for the rotational links of the modules, a three-dimensional configuration will be feasible. The feasibility study of the uni-drive modular robot shown in Fig. 8 using a central rotating shaft along with the modules has been already investigated in previous studies at the University of Waterloo.[15–17,22,23]

To obtain the total kinetic and potential energy of the system, we first derive the Cartesian coordinates of the center of masses in terms of generalized coordinates. Kinetic and potential energy can then be obtained in terms of generalized coordinates. Considering Rayleigh's dissipation function and the Euler–Lagrange equation, the $2n$ equations of motion in the form of an SEF can be derived as follows:

- Translational equations

$$
\begin{aligned}
&(m_1+m_2)\sum_{i=k+1}^{n}\sum_{j=1}^{i-1}\left(\dot{\Omega}_j^1\cos q_{k1}+\dot{\Omega}_j^2\sin q_{k1}\right)\\
&\quad+\sum_{i=k+1}^{n}\left(\dot{\Omega}_i^3\cos q_{k1}+\dot{\Omega}_i^4\sin q_{k1}\right)\\
&\quad+m_2\sum_{i=1}^{k-1}\left(\dot{\Omega}_i^1\cos q_{k1}+\dot{\Omega}_i^2\sin q_{k1}\right)+(n-k)\\
&\quad\times(m_1+m_2)\,g\sin q_{k1}+m_2 g\sin q_{k1}+m_2\ddot{q}_{k2}\\
&\quad-m_2 q_{k2}\dot{q}_{k1}^2+c_2\dot{q}_{k2}=Q_{k2}\quad k=1,\ldots,n,
\end{aligned}
\tag{5}
$$

- Rotational equations[3]

$$
\begin{aligned}
&(I_1+I_2)\ddot{q}_{k1}+(m_1+m_2)\sum_{i=k+1}^{n}\sum_{j=1}^{i-1}\left\{-(q_{k2}+d)\dot{\Omega}_j^1\sin q_{k1}\right.\\
&\quad\left.+(q_{k2}+d)\dot{\Omega}_j^2\cos q_{k1}\right\}\\
&\quad+\sum_{i=k+1}^{n}\left\{-(q_{k2}+d)\dot{\Omega}_i^3\sin q_{k1}+(q_{k2}+d)\dot{\Omega}_i^4\cos q_{k1}\right\}\\
&\quad+\sum_{i=1}^{k-1}\left\{-(m_1 l+m_2 q_{k2})\dot{\Omega}_i^1\sin q_{k1}+(m_1 l+m_2 q_{k2})\right.\\
&\quad\left.\times\dot{\Omega}_i^2\cos q_{k1}\right\}+(n-k)(m_1+m_2)g(q_{k2}+d)\\
&\quad\times\cos q_{k1}+(m_1 l+m_2 q_{k2})g\cos q_{k1}+\left(m_1 l^2+m_2 q_{k2}^2\right)\\
&\quad\times\ddot{q}_{k1}+2m_2 q_{k2}\dot{q}_{k2}\dot{q}_{k1}+\tfrac{\partial E_c}{\partial\dot{q}_{k1}}=Q_{k1}\qquad k=1,\ldots,n,
\end{aligned}
\tag{6}
$$

[3] The complete derivation of SEF Eqs. (5) and (6) can be found in ref. [22].

https://doi.org/10.1017/S0263574709005670 Published online by Cambridge University Press

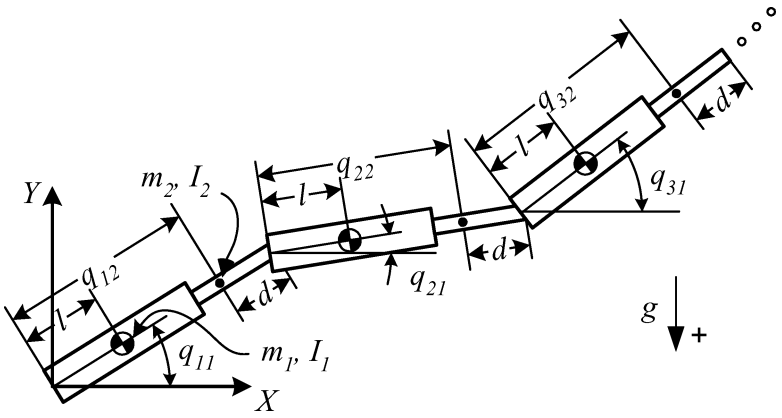

Fig. 8. The coordinates description of the planar modular robot.

where $\frac{\partial E_c}{\partial \dot{q}_{k1}}$ and generalized forces (actuator torques and forces) are defined as

$$\frac{\partial E_c}{\partial \dot{q}_{k1}} = \begin{cases} c_1\dot{q}_{11} & \text{for } k = n = 1 \\ 2c_1\dot{q}_{k1} - c_1\dot{q}_{(k-1)1} - c_1\dot{q}_{(k+1)1} & \text{for } 1 \le k < n,\ n \ne 1 \\ c_1\dot{q}_{n1} - c_1\dot{q}_{(n-1)1} & \text{for } k = n,\ n \ne 1, \end{cases} \tag{7}$$

$$Q_{ij} = \begin{cases} \tau_i - \tau_{i+1} & i = 1, \ldots, n \\ f_i & i = 1, \ldots, n. \end{cases} \tag{8}$$

In the SEF Eqs. (5) and (6), $\dot{\Omega}_i^j$ are the time derivatives of

$$\begin{aligned} \Omega_j^1 &= -\dot{q}_{j1}(q_{j2} + d)\sin q_{j1} + \dot{q}_{j2}\cos q_{j1}, \\ \Omega_j^2 &= \dot{q}_{j1}(q_{j2} + d)\cos q_{j1} + \dot{q}_{j2}\sin q_{j1}, \\ \Omega_i^3 &= -m_1 l\dot{q}_{i1}\sin q_{i1} + m_2(\dot{q}_{i2}\cos q_{i1} - q_{i2}\dot{q}_{i1}\sin q_{i1}), \\ \Omega_i^4 &= m_1 l\dot{q}_{i1}\cos q_{i1} + m_2(\dot{q}_{i2}\sin q_{i1} + q_{i2}\dot{q}_{i1}\cos q_{i1}). \end{aligned} \tag{9}$$

As seen in the SEF, $2n$ equations are generated automatically to define the dynamic behavior of the uni-drive modular robot. The validation of Eqs. (5) and (6) has been also proved using the conservation of energy principle and a Newton–Euler algorithm based on the Denavit–Hartenberg (DH) notation.[22]

3.2. Integrating Mechanical Drive Dynamics into SEF

In order to apply the SEF given by Eqs. (5) and (6) to a uni-drive modular robot, the dynamics of the mechanical drive Eqs. (2) to (4) should be considered. In this model, f_{sol} can be related to the PWM signal, u by a nonlinear first-order differential equation, and the state space model of Eqs. (2)–(4) can then be obtained as:

$$\begin{aligned} \dot{x}_1 &= F_{sol}(u, x_1), \\ k_1\ddot{x}_2 + k_2\dot{x}_2 + k_3 x_2 &= x_1, \\ k_4\ddot{x}_3 + k_5(\dot{x}_3 - \dot{x}_4) + k_6(x_3 - x_4) + k_7\dot{x}_3 &= k_8 x_1, \\ k_9\ddot{x}_4 + k_5(\dot{x}_4 - \dot{x}_3) + k_6(x_4 - x_3) + k_{10}\dot{x}_4 &= k_{11}(\omega_i - \dot{x}_4), \end{aligned} \tag{10}$$

where k_{1-11} are the clutch and load parameters, and u and ω_i are the PWM signal and clutch input speed, respectively. The first equation in Eqs. (10) represents the nonlinear model of the clutch solenoid force. The last three equations in Eqs. (10) are associated with Eqs. (2), (3), and (4), respectively. This model can represent the bidirectional motion of the load by switching the sign of ω_i. The left-hand side of the fourth equation in Eqs. (10) includes the dynamics of the load to which the clutch is attached, and its right-hand side represents the actuator force/torque. In fact, to apply the SEF to the planar uni-drive modular robot with n modules, the first three equations in Eqs. (10) must be added to both Eq. (5) and Eq. (6) and the actuator force/torque replaced by the associated expression in Eqs. (10). In this case, the total number of equations in the SEF increases to $8n$. The equations for translational motion are:

$$\begin{aligned} &(m_{1eff} + m_{2eff}) \sum_{i=k+1}^{n} \sum_{j=1}^{i-1} \left(\dot{\Omega}_j^1 \cos q_{k1} + \dot{\Omega}_j^2 \sin q_{k1}\right) \\ &\quad + \sum_{i=k+1}^{n} \left(\dot{\Omega}_i^3 \cos q_{k1} + \dot{\Omega}_i^4 \sin q_{k1}\right) \\ &\quad + m_{2eff} \sum_{i=1}^{k-1} \left(\dot{\Omega}_i^1 \cos q_{k1} + \dot{\Omega}_i^2 \sin q_{k1}\right) + (n - k) \\ &\quad \times (m_{1eff} + m_{2eff}) g \sin q_{k1} + m_{2eff} g \sin q_{k1} \\ &\quad + m_{2eff}\ddot{q}_{k2} - m_{2eff} q_{k2}\dot{q}_{k1}^2 + c_{2eff}\dot{q}_{k2} = k'_{11}(\omega_i - \dot{q}_{k2}), \end{aligned} \tag{11a}$$

$$k_4\ddot{x}_{k3} + k_5(\dot{x}_{k3} - \dot{q}_{k2}) + k_6(x_{k3} - q_{k2}) + k_7\dot{x}_{k3} = k_8 x_{k1}, \tag{11b}$$

$$k_1\ddot{x}_{k2} + k_2\dot{x}_{k2} + k_3 x_{k2} = x_{k1}, \tag{11c}$$

$$\dot{x}_{k1} = F_{sol}(u_k, x_{k1}), \qquad k = 1, \ldots, n. \tag{11d}$$

The equations for rotational motion are:

$$\begin{aligned} &(I_{1eff} + I_{2eff})\ddot{q}_{k1} + (m_{1eff} + m_{2eff}) \sum_{i=k+1}^{n} \\ &\quad \sum_{j=1}^{i-1} \left\{ -(q_{k2} + d)\dot{\Omega}_j^1 \sin q_{k1} + (q_{k2} + d)\dot{\Omega}_j^2 \cos q_{k1} \right\} \end{aligned}$$

https://doi.org/10.1017/S0263574709005670 Published online by Cambridge University Press

$$+\sum_{i=k+1}^{n}\{-(q_{k2}+d)\dot{\Omega}_i^3\sin q_{k1}+(q_{k2}+d)\dot{\Omega}_i^4\cos q_{k1}\}$$
$$+\sum_{i=1}^{k-1}\{-(m_{1eff}l+m_{2eff}q_{k2})\dot{\Omega}_i^1\sin q_{k1}$$
$$+(m_{1eff}l+m_{2eff}q_{k2})\dot{\Omega}_i^2\cos q_{k1}\}+(n-k)$$
$$\times\left(m_{1eff}+m_{2eff}\right)g(q_{k2}+d)\cos q_{k1}$$
$$+\left(m_{1eff}l+m_{2eff}q_{k2}\right)g\cos q_{k1}+(m_{1eff}l^2+m_{2eff}q_{k2}^2)$$
$$\times\ddot{q}_{k1}+2m_{2eff}q_{k2}\dot{q}_{k2}\dot{q}_{k1}+\frac{\partial E_c}{\partial\dot{q}_{k1}}=k_{11}(\omega_i-\dot{q}_{k1}), \tag{12a}$$

$$k_4\ddot{y}_{k3}+k_5(\dot{y}_{k3}-\dot{q}_{k1})+k_6(y_{k3}-q_{k1})+k_7\dot{y}_{k3}=k_8y_{k1}, \tag{12b}$$

$$k_1\ddot{y}_{k2}+k_2\dot{y}_{k2}+k_3y_{k2}=y_{k1}, \tag{12c}$$

$$\dot{y}_{k1}=F_{sol}(v_k,y_{k1}),\qquad k=1,\ldots,n. \tag{12d}$$

Notice that in Eqs. (11) and (12), I_1, I_2, m_1, m_2, c_1, and c_2 are replaced by I_{1eff}, I_{2eff}, m_{1eff}, m_{2eff}, c_{1eff}, and c_{2eff}, respectively, to include the effect generated by the clutch mass and inertia in each joint. k'_{11} and k_{11} represent force and torque coefficients, respectively, and $\frac{\partial E_c}{\partial\dot{q}_{k1}}$ and $\dot{\Omega}_i^j$ are defined in Eq. (7) and as the time derivative of Eq. (9). In Eqs. (11) and (12), $x_{k/s}$, $y_{k/s}$, u_k, and v_k represent the clutch variables and PWM signals, respectively.

4. Control of Uni-Drive Modular Robots

In Section 2, the control structure of a uni-drive modular robot using local controllers and path planner was introduced. For implementation of this structure, the articulated uni-drive modular robot shown in Fig. 8 (which has no limit on the number of modules used) is considered. To achieve a robust design methodology for local controllers, the key strategy is to combine the independent joint control of manipulators and the theory of variable structure (VS) systems.

In order to design local controllers, here we use independent joint control (IJC) in which each axis of the manipulator is controlled as a single-input/single-output (SISO) system. The actuator dynamics are considered as a SISO system, and any coupling effect due to the motion of the other links is either ignored or treated as a disturbance. To apply independent joint control to a uni-drive modular robot, SEF Eqs. (5) and (6) which includes the nonlinear inertia, centripetal, Coriolis, and gravitational coupling effects due to the motion of the manipulator and actuator dynamics are considered separately. In Eqs. (5) and (6), Q_{k1} and Q_{k2} are the joints' torque and force, respectively. In uni-drive modular robots the actuator dynamics are replaced by mechanical drive dynamics. The dynamic model of the mechanical drive is given by Eq. (10). The first three equations in Eqs. (10) represent the dynamics of the magnetic circuit and motions of the control ring of the SWC. For now, these dynamics can be ignored if we assume ideal switching occurs without any delay. Later on, we will compensate for this assumption in the design of local controllers. Furthermore, the last equation can be simplified by assuming that the inertia of the control ring can be ignored when compared to the inertia of the modules. Based on these assumptions, the mechanical drive dynamic for revolute joints is given by

$$J_{eff1}\ddot{\theta}_{k1}+B_{eff1}\dot{\theta}_{k1}=\tau_{k1}-r_{k1}Q_{k1};\quad k=1,\ldots,n, \tag{11}$$

and for translational joints is given by

$$J_{eff2}\ddot{\theta}_{k2}+B_{eff2}\dot{\theta}_{k2}=\tau_{k2}-r_{k2}Q_{k2};\quad k=1,\ldots,n, \tag{12}$$

where $\dot{\theta},\theta,J_{eff},B_{eff}$, and r_k represent the angular position and velocity of the SWC, effective inertia, damping coefficient and gear ratio of the mechanical drives, respectively. Index 1 refers to the mechanical drive associated with rotational joints while index 2 refers to the mechanical drive associated with translational joints. In Eqs. (11) and (12), τ_{k1} and τ_{k2} are the torque and force produced by mechanical drives (i.e., virtual viscous torque and force). Considering Eqs. (10) they can be written as

$$\tau_{k1}=c(\omega_i-\dot{\theta}_{k1}), \tag{13}$$
$$\tau_{k2}=c(\omega_i-\dot{\theta}_{k2}), \tag{14}$$

where c represents a virtual damping coefficient. Equations (5) and (6) associated with Eqs. (11) and (12) form the skeleton of the independent joint control for the uni-drive modular robot.

4.1. Robust controller design for robot manipulators

The PWM technique used to control the clutches in the mechanical drives gives a VS nature to the uni-drive modular robot dynamics. One of the best controller design methodologies to control VS systems is sliding mode control.[24] For a class of nonlinear systems, sliding mode control addresses the following problem: given the extent of parametric uncertainty (such as imprecision of inertias, geometry, loads) and of disturbances (such as Coulomb or viscous friction) and the frequency range of unmodeled dynamics (such as unmodeled structural modes, neglected time delays), design a nonlinear feedback controller to achieve optimal tracking precision, in a suitable sense. This methodology provides a decoupled set of equations which are very applicable to the control of manipulators. By using a decoupled approach for controlling each DOF of a manipulator, simpler and more tractable controllers can be designed.

To illustrate some of the advantages of the sliding mode approach to deal with nonlinear systems with uncertainties and similar equations as those in Eqs. (11) and (12), we consider a nonlinear time invariant system given by

$$\dot{x}_1=x_2$$
$$\dot{x}_2=ax_2-bu+d\sin(x_1)+z(t),\quad a,\ b>0 \tag{15}$$
$$x^T=(x_1,x_2).$$

In this system, u is the main input, and the first two terms of the second equation describe a linear system. The last two

https://doi.org/10.1017/S0263574709005670 Published online by Cambridge University Press

terms show additional nonlinearity and a disturbance input $z(t)$. A VS control law is of the form

$$u = \psi_1 x_1 + \psi_2 x_2 + \psi_3 x_3, \quad x_3 \equiv z, \tag{16}$$

where the coefficients ψ_i are discontinuous,

$$\psi_i = \begin{cases} \alpha_i \text{sgn}(b), & \text{if } x_i s > 0 \\ -\alpha_i \text{sgn}(b), & \text{if } x_i s < 0 \end{cases} \quad \alpha_i > 0, i = 1, 2, 3, \tag{17}$$

and $s = 0$ defines the switching line, that is,

$$s = \lambda x_1 + x_2 = 0, \quad \lambda > 0. \tag{18}$$

We select α_i such that s and $\dot{s}$ have opposite signs in the neighborhood of $s = 0$, that is,

$$\dot{s}s < 0. \tag{19}$$

The sliding mode occurs on $s = 0$ and the motion continues along the switching line in Eq. (18). Another expression for Eq. (19) is

$$\frac{1}{2}\frac{\text{d}}{\text{d}t}s^2 \le -\eta |s| \quad \text{or} \quad \dot{s} \le -\eta \text{sgn}(s), \tag{20}$$

where η is a design parameter which adjusts the approach speed of the system trajectories to the switching line. When the system of Eq. (17) is on the switching line, its trajectories $(x_1(t), x_2(t))$ satisfy $s = \lambda x_1(t) + x_2(t) = 0$, which implies that $x_1(t)$ is governed by the equation

$$\dot{x}_1 = -\lambda x_1. \tag{21}$$

This is called the equation of the sliding mode. It is a reduced order system which represents the original system of Eq. (15) when on the switching line. Initially, the equation of the sliding mode was obtained by the equivalent control method proposed by Utkin.[26] According to this method, u is solved for the algebraic equation $\dot{s} = 0$. By taking the derivative of Eq. (18) and using Eq. (15), $\dot{s}$ becomes

$$\dot{s} = \lambda x_2 + a x_2 - b u + d \sin(x_1) + z(t) = 0. \tag{22}$$

By solving Eq. (22) for u_{eq} and substituting in Eq. (15), Eq. (21) is obtained by restricting x_1, x_2 to satisfy Eq. (18). Observing that Eq. (21) depends only on λ, we see that sliding mode does not depend on system parameters a and b, or on nonlinearity $d \sin(x_1)$, or disturbance $z(t)$. This clearly exhibits the insensitivity with respect to system parameters and the disturbance rejection capability of sliding mode control. Furthermore, Eq. (21) has an eigenvalue equal to $-\lambda$. Our earlier choice of positive values of λ in Eq. (18) insures asymptotic stability. The response speed in sliding mode is determined by λ, which is a design parameter.

Let us assume that the parameters a, b, and d are unknown but that their bounds M_1, M_2, and M_3 are known; that is, $|a| < M_1$, $M_2 < |b| < \infty$, and $|d| < M_3$. Furthermore, we assume that the sign of b is known and disturbance $z(t)$ is available for measurement. Since $-|x_1| < \sin(x_1) < |x_1|$, then the sliding mode condition of Eq. (19) is satisfied when

$$\alpha_1 > \frac{M_3}{M_2}, \quad \alpha_2 > \frac{\lambda + M_1}{M_2}, \quad \alpha_3 > \frac{1}{M_2}. \tag{23}$$

Thus to determine the α_i in Eq. (17), we only need to know the bounds M_i on the system parameters. It may appear that since the disturbance $z(t)$ is measurable, a feedforward term with constant gain added in the control is sufficient to remove its influence. Nevertheless, a switching gain is necessary due to parameter uncertainty in b.

When sliding occurs, the VS control of Eq. (16) is ideally switched at an infinite frequency. In reality, the control is switched at a finite frequency and the corresponding trajectories chatter with respect to the switching plane. We refer to these trajectories as nonideal sliding mode. It can be shown that if u_{eq} is unique, the nonideal sliding mode is close to the ideal sliding mode defined by Eq. (21). Given a parameter Δ depending on the type and size of imperfections (switching hysteresis or delay, finite slope switching, neglected small time constants, etc.) there exists a positive number H such that the difference between the ideal $x(t)$ and nonideal sliding mode $\tilde{x}(t)$ is bounded by

$$\|x(t) - \tilde{x}(t)\| \le H\Delta, \tag{24}$$

for all $t \in [t_1, \infty)$ providing that at $t = t_1$, the state is within Δ of the switching line, that is,

$$\|s(t_1)\| \le \Delta. \tag{25}$$

Chattering must be eliminated for the controller to perform properly. This can be achieved by smoothing out the control discontinuity in a thin boundary layer neighboring the switching line:

$$B(t) = \{x, |s(x, t) \le \phi|\}, \quad \phi > 0, \tag{26}$$

where ϕ is the boundary layer thickness, and $\varepsilon = \phi/\lambda$ is the boundary layer width, as shown in Fig. 9 for a second-order

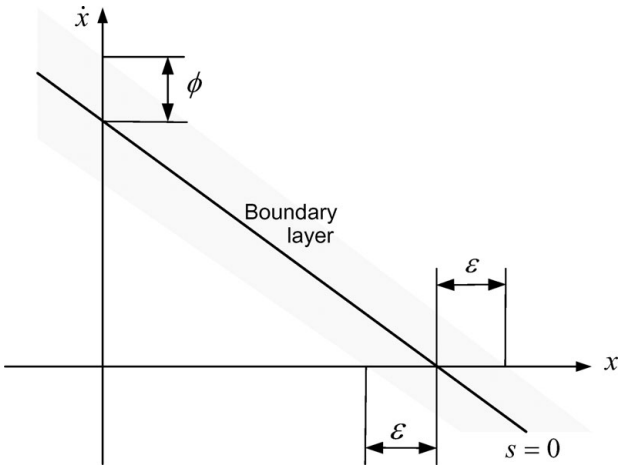

Fig. 9. Smoothing out the control discontinuity using a thin boundary layer.

https://doi.org/10.1017/S0263574709005670 Published online by Cambridge University Press

system.[25] In other words, outside $B(t)$, we choose control law u as before (i.e., satisfying sliding condition of Eq. (20)), which guarantees that the boundary layer is attractive, hence invariant. As a result of this, all trajectories starting inside $B(t=0)$ remain inside $B(t)$ for all $t \geq 0$; and we then interpolate u inside $B(t)$. To implement this change in the expression of Eq. (20), the term $\text{sgn}(s)$ is replaced by $\text{sat}(s/\phi)$. This leads to tracking within a guaranteed precision ε (rather than perfect tracking), and more generally guarantees that for all trajectories starting inside $B(t=0)$

$$\forall\, t \geq 0,\ \|x(t) - x_d(t)\| \leq 2\lambda\varepsilon, \tag{27}$$

where $x(t) - x_d(t)$ is the tracking error. For more details on this issue, the reader is referred to ref. [25, Chapter 7].

Summarizing the results obtained from the above example, the local controller design procedure consists of two steps. First, a feedback control law u is selected so as to verify a sliding condition of Eq. (20). Considering the presence of modeling errors and disturbances, chattering is unavoidable. Chattering is undesirable in practice because it involves high control activity, and further, it may excite high-frequency dynamics neglected in the course of modeling (such as unmodeled structural modes and neglected time delays). Thus, in a second step, a discontinuous control law u is suitably smoothed to achieve an optimal trade-off between control bandwidth and tracking precision. While the first step accounts for parametric uncertainty, the second steps achieves robustness to high-frequency unmodeled dynamics.

4.2. Design of local controllers: independent joint control and theory of VS systems

In this section, we combine the independent joint control and theory of VS systems to develop a controller design procedure for uni-drive modular robots. To begin this discussion, for simplicity we drop indices 1 and 2 and rewrite Eqs. (11) and (12) that are obtained from the independent joint control approach as:

$$J_{eff}\ddot{\theta}_k + B_{eff}\dot{\theta}_k = u_k - d_k; \quad k = 1, \ldots, n. \tag{28}$$

For a particular link, u_k is the input torque provided by its mechanical drive and d_k is the disturbance load $r_k Q_k$ received from the inertia and different accelerations of other links. We consider the following set point regulation problem: assuming $\theta \equiv p$ and $\dot{\theta} \equiv v$, for the given initial states $p(t_0)$, $v(t_0)$, and desired position p_d, velocity $v_d = 0$, find a discontinuous feedback control $u(p, v)$ such that $p(t) \to p_d$ and $v(t) \to 0$. In terms of the position error $e(t) = p(t) - p_d$, our goal is to nullify the error $e(t)$. Accordingly, the state space representation of Eq. (28) is

$$\begin{aligned} \dot{e}_k &= v_k, \\ \dot{v}_k &= -a v_k + b u_k - d'_k;\ k = 1, \ldots, n, \end{aligned} \tag{29}$$

where $a = \frac{B_{eff}}{J_{eff}}$, $b = \frac{1}{J_{eff}}$, and $d'_k = \frac{d_k}{J_{eff}}$. From the similarity between Eqs. (15) and (29), and assuming that the bound of system parameters and disturbances are known, we can readily come up with the sliding mode design for Eq. (29). For this case, the VS control law has a fixed amplitude and is defined as

$$u_k = \psi_{1k}\omega_i \text{sgn}(v_k) + \psi_{2k} M_{3k} \text{sgn}(d'_k), \tag{30}$$

where $|v_k| \leq \omega_i$, $|d'_k| < M_{3k}$, and the coefficients ψ_{1k} and ψ_{2k} are

$$\psi_{1k} = \begin{cases} -\alpha_{1k} & \text{if } v_k s_k > 0 \\ \alpha_{1k} & \text{if } v_k s_k < 0 \end{cases}, \quad \alpha_{1k} > 0, \tag{31}$$

$$\psi_{2k} = \begin{cases} -\alpha_{2k} & \text{if } d'_k s_k > 0 \\ \alpha_{2k} & \text{if } d'_k s_k < 0 \end{cases}, \quad \alpha_{2k} > 0,$$

and switching lines

$$s_k = \lambda_k e_k + v_k = 0, \quad \lambda_k > 0, \tag{32}$$

then the sliding mode condition $\dot{s}_k s_k < 0$ is satisfied for $k = 1, \ldots, n$ when

$$\alpha_{1k} > \frac{\lambda_k - M_1}{M_2}, \quad \alpha_{2k} > \frac{1}{M_2}, \tag{33}$$

where

$$M_1 < a, \quad M_2 < b < \infty, \quad \lambda_k > a, \tag{34}$$

and for $\dot{s}_k = 0$, u_{eq} can be found as

$$u_{eq} = \frac{1}{b}((a - \lambda_k)v_k + d'_k). \tag{35}$$

The validity of the above design can be easily shown by examining all possible cases that yield the sign of s_k and $\dot{s}_k$ and hereby $\dot{s}_k s_k$. Considering Eqs. (29), (30), and (32) we obtain $\dot{s}_k$ as

$$\dot{s}_k = (\lambda_k - a)v_k + b(\psi_{1k}\omega_i \text{sgn}(v_k) + \psi_{2k} M_{3k} \text{sgn}(d'_k)) - d'_k. \tag{36}$$

There are six states with a combination of different signs for s_k, v_k, and d'_k. In each of these cases, using Eqs. (31) and (33), the sign of $\dot{s}_k$ can be found and must be opposite to the sign of s_k to verify the design. The six states and proper values for ψ_{1k} and ψ_{2k} are

$$\begin{aligned} &\text{if } s_k > 0,\ v_k > 0,\ d'_k > 0 \text{ and } -\alpha_{1k},\ -\alpha_{2k} \text{ then } \dot{s}_k < 0, \\ &\text{if } s_k > 0,\ v_k < 0,\ d'_k > 0 \text{ and } \alpha_{1k},\ -\alpha_{2k} \text{ then } \dot{s}_k < 0, \\ &\text{if } s_k > 0,\ v_k > 0,\ d'_k < 0 \text{ and } -\alpha_{1k},\ \alpha_{2k} \text{ then } \dot{s}_k < 0, \\ &\text{if } s_k < 0,\ v_k < 0,\ d'_k < 0 \text{ and } -\alpha_{1k},\ -\alpha_{2k} \text{ then } \dot{s}_k > 0, \\ &\text{if } s_k < 0,\ v_k > 0,\ d'_k < 0 \text{ and } \alpha_{1k},\ -\alpha_{2k} \text{ then } \dot{s}_k > 0, \\ &\text{if } s_k < 0,\ v_k < 0,\ d'_k > 0 \text{ and } -\alpha_{1k},\ \alpha_{2k} \text{ then } \dot{s}_k > 0. \end{aligned} \tag{37}$$

Considering Eq. (37), the expression in Eq. (30) for u_k can be simplified to

$$u_k = -(\alpha_{1k}\omega_i + \alpha_{2k} M_{3k})\text{sgn}(s_k). \tag{38}$$

https://doi.org/10.1017/S0263574709005670 Published online by Cambridge University Press

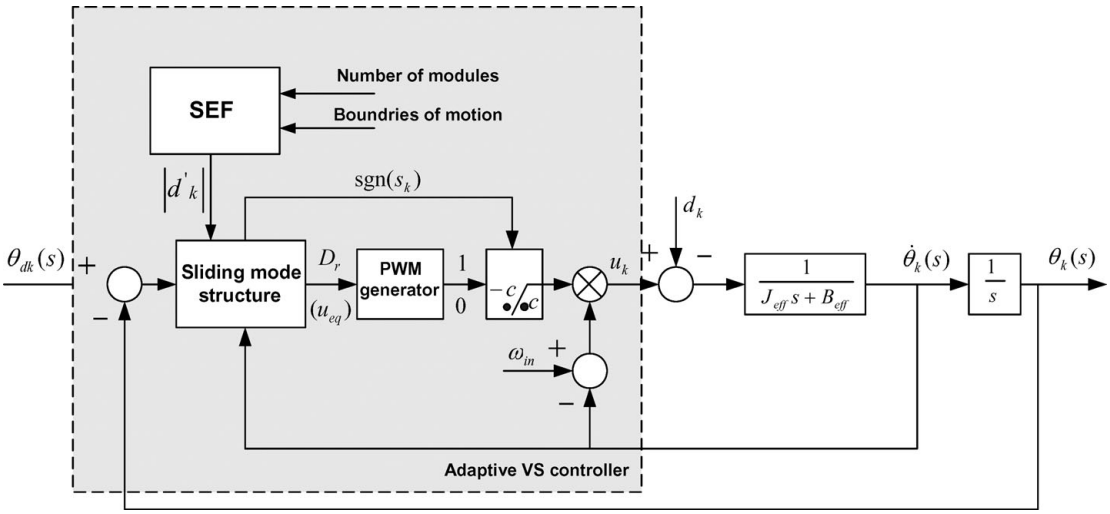

Fig. 10. Adaptive VS local controller for the uni-drive modular robots.

5. Simulation

In this section, the performance of local controllers will be studied via simulation.

5.1. Adaptive VS local controller

Figure 10 shows an adaptive VS controller used as local controller for each joint in the uni-drive modular robot. The main substructures of the local controller are the SEF introduced in previous sections, and the sliding mode structure and PWM generator. The inputs to the sliding mode structure are $|d'_k|$ generated by the SEF, the error in position and output velocity of the mechanical drive, while its outputs are the duty ratio D (u_{eq}, when the system trajectory reaches the switching line, an assumption which is valid when the PWM frequency is relatively high) to the PWM generator and the sign of s_k. By knowing the number of modules and their boundaries of motion such as range of travel, velocity, and acceleration, the SEF will automatically calculate the $|d'_k|$ as a main input parameter for the design of the sliding mode structure in Eq. (35). Using the PWM generator and sign of s_k, the virtual damping coefficient of the mechanical drive switches between either 0 and c or 0 and $-c$. Then the output of the mechanical drive u_k is a positive or negative torque based upon the sign of s_k. The mechanical drive torque is affected by the disturbance d_k (representing the dynamics of the robot structure) and the result causes the mechanical drive to rotate.

To study the performance of the designed VS controller shown in Fig. 10, we consider a mechanical drive whose parameters are

$$J_{eff} = 0.01\,\mathrm{kgm}^2,\ B_{eff} = 0.1\,\mathrm{Ns/m}. \tag{39}$$

The values for a and b used in Eq. (29) are therefore 10 and 100 respectively. For this case we consider a random torque disturbance d_k with $|d_k| < 2.5$ N.m and a mean value of zero and variance of one; thus $|d'_k| < 250$ and $M_{3k} = 300$. The input speed to the mechanical drive is assumed to be 30 rad/sec. Using these values and assumptions, we are able to design the VS controller parameters in Eqs. (33) and (34)

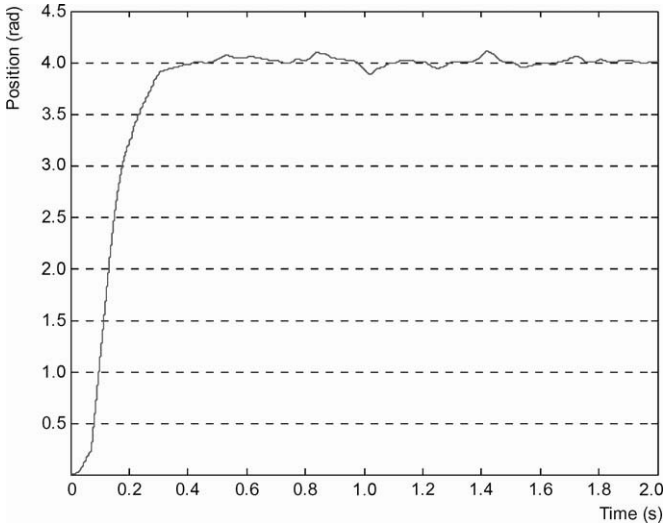

Fig. 11. Step response of a mechanical drive with VS controller in the presence of disturbance, $|d_k| < 2.5$.

as

$$M_1 = 5,\ M_2 = 50,\ \text{and}\ \lambda_k = 15,$$
$$\alpha_{1k} = 0.25,\ \alpha_{2k} = 0.03. \tag{40}$$

Considering (40) and (38), we find the amplitude of u_k as:

$$|u_k| = \alpha_{1k}\omega_i + \alpha_{2k}M_{3k} = 16.5. \tag{41}$$

Using the block diagram shown in Fig. 10, the simulation results of the mechanical drive are depicted in Fig. 11. For this simulation, the set point and the PWM frequency are 4 rad and 10 Hz., respectively. It should be noted that if we consider a gear ratio of r for the mechanical drive, the real position of the joint attached to the mechanical drive is obtained as $r\theta$ while the real disturbance would be d_k/r.

In Fig. 12(a), (b), and (c), $s(x)$, the disturbance and the PWM signals are shown, respectively. The value of Δ in Eq. (25) can be measured from Fig. 12(a) to be equal to 5. According to Eq. (24) and Fig. 11, the maximum positioning

https://doi.org/10.1017/S0263574709005670 Published online by Cambridge University Press

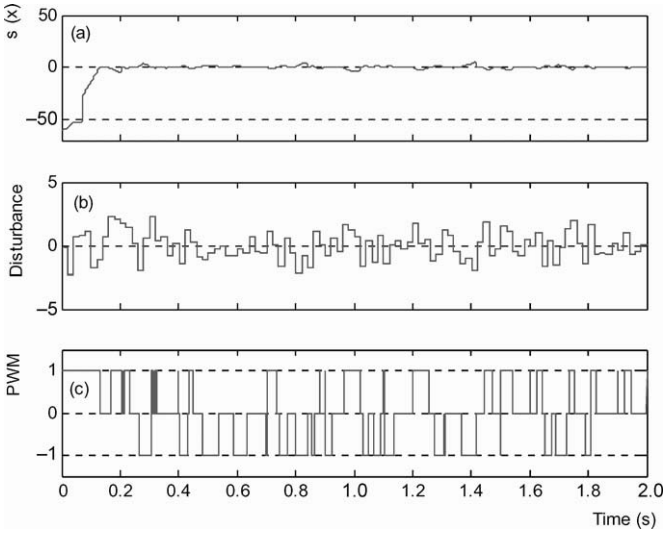

Fig. 12. Positioning control: (a) switching line (b) disturbance $|d_k| < 2.5$, and (c) PWM.

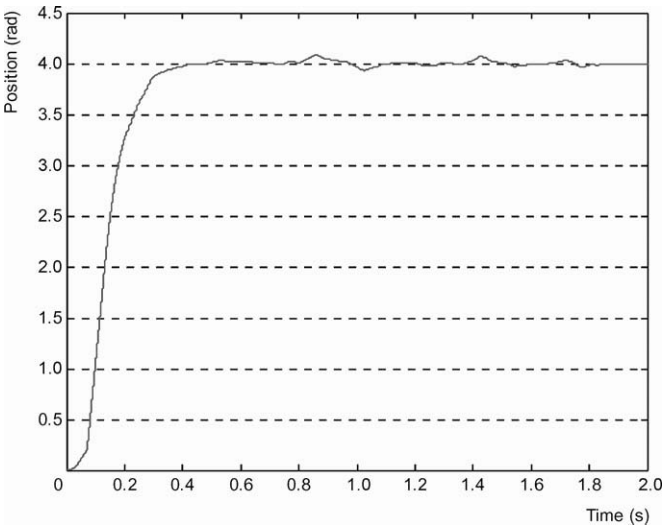

Fig. 13. Time response of a mechanical drive with VS controller in the presence of disturbance, $|d_k| < 1.7$.

error $H\Delta$ is 0.12 in the presence of the disturbance. Hence, the constant H is calculated to be equal to 0.024 and if Δ is considered proportional to disturbance d_k, the proportionality coefficient is found to be 2. Using the values of H and Δ in the above example, we are able to predict the position error in different cases. For instance, if $|d_k| < 1.7$ then $\Delta = 3.4$ and the position error $H\Delta = 0.0816$. In Fig. 13, the step response of the mechanical drive is shown while the disturbance is $|d_k| < 1.7$. In Fig. 14(a), (b), and (c), $s(x)$, the disturbance and the PWM signals are shown for this case, respectively. Figures 13 and 14(a) verify these predictions by showing a position error of 0.08 and $\Delta = 3.2$.

6. Conclusions

In this paper, we have studied and developed a stability analysis and controller design method for uni-drive modular robots. The new modular robot benefits from much lighter modules due to the uni-drive concept. The main element

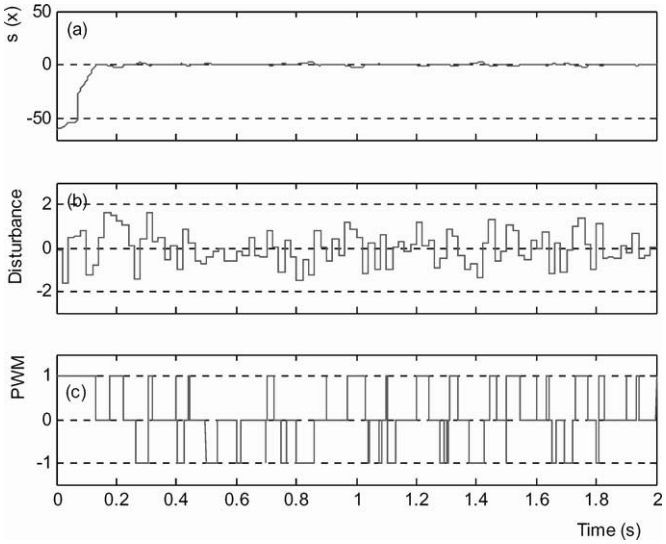

Fig. 14. Positioning control: (a) switching line (b) disturbance $|d_k| < 1.7$, and (c) PWM.

of a uni-drive modular robot is a mechanical drive capable of providing a variable bidirectional speed from a constant unidirectional input velocity. The design of the mechanical drive was reviewed and its mathematical model was integrated into the SEF which is very useful for generating the dynamics of uni-drive modular robots based only on the number of modules.

The design of local controllers was achieved based upon blending of independent joint control and theory of VS systems. Based on this design, each axis of the manipulator is controlled as a SISO system. The actuator dynamics are considered as a SISO system and any coupling effects due to the motion of the other links is either ignored or treated as a disturbance. Sliding mode was used to deal with the control of the mechanical drive as a VS systems. Sliding mode control addresses problems such as parametric uncertainties, disturbances, and the frequency range of unmodeled dynamics to achieve optimal tracking precision, in a suitable sense.

Acknowledgments

The authors would like to acknowledge the financial support of the Natural Sciences and Engineering Research Council of Canada (NSERC).

References

1. R. Ambrose, Design, Construction and Demonstration of Modular, Reconfigurable Robots *Ph.D. Thesis* (Austin, TX: University of Texas, 1991).
2. O. Chocron, "Evolutionary design of modular robotic arms," *Robotica* **26**(3), 323–330 (May–Jun. 2008).
3. G. J. Liu, S. Abdul and A. A. Goldenberg, "Distributed control of modular and reconfigurable robot with torque sensing," *Robotica* **26**(1), 75–84 (Jan.–Feb. 2008).
4. Y. Q. Fei, X. F. Zhao and L. B. Song, "A method for modular robots generating dynamics automatically," *Robotica* **19**(1), 59–66 (Jan.–Feb. 2001).
5. I. Chen and G. Yang, "Configuration Independent Kinematics for Modular Robots," *IEEE Conference on Robotics and Automation*, Minneapolis, MN (1996) pp. 1440–1445.

https://doi.org/10.1017/S0263574709005670 Published online by Cambridge University Press

6. R. Cohen, M. Lipton, M. Dai and B. Benhabib, "Conceptual design of a modular robot," *ASME J. Mech. Des.* **114**, 117–125, (Mar. 1992).
7. T. Fukuda and S. Nakagawa, "Dynamically Reconfigurable Robotic System," *IEEE International Conference on Robotics and Automation*, Philadelphia, PA (1988) pp. 1581–1586.
8. C. Paredis, H. Brown, R. Casciola, J. Moody and P. Khosla, "A Rapidly Deployable Manipulator System," *International Workshop on Some Critical Issues in Robotics*, Singapore (1995) pp. 175–185.
9. K. Wurst, "The Conception and Construction of a Modular Robot System," *International Symposium on Industrial Robotics*, San Francisco, CA (1986) pp. 37–44.
10. T. Matsumaru, "Design and Control of the Modular Robot System: Tomms," *IEEE International Conference on Robotics and Automation*, Nagoya, Aichi, Japan (1995) pp. 2125–2131.
11. D. Schmitz, P. Khosla and T. Kanade, "The CMU Reconfigurable Modular Manipulator System," *Technical Report CMU-RI-TR-88-7* (Carnegie Mellon University, 1988).
12. Y. Ishii, T. Fukuzawa, Y. Ichikawa, M. Suzuki, S. Naito and N. Iwatsuka, "A Joint Connection Mechanism and Control System for a Reconfigurable Manipulator," *SICE '92*, Kobe, Japan (1992) pp. 1095–1098.
13. M. Yim, W. Shen, B. Salemi, D. Rus, M. Mall, H. Lipson, E. Klavins, G. S. Chirikjian, "Modular self-reconfigurable robot systems: Challenges and opportunities for the future," *IEEE Robot. Autom. Mag.* **14**(1), 43–52 (Mar. 2007).
14. M. Yim, "A Reconfigurable Modular Robot with Many Modes of Locomotion," *Proceedings of the JSME International Conference on Advanced Mechatronics*, Tokyo, Japan, (1993) pp. 1095–1098.
15. H. Karbasi, J. P. Huissoon and A. Khajepour, "Experimental and theoretical analysis of a uni-drive modular robot: Design and Modeling," *Proceedings of DETC/CIE'02: 27th ASME biennial mechanisms and robotics conference*, CDRom-DETC2002/MECH-34351, Montreal, Canada (Sep. 29–Oct. 2, 2002).
16. H. Karbasi, A. Khajepour, J. P. Huissoon and S. J. Park, "A New Modular Robot: Uni-Drive with Pulse Width Modulation Control," *Proceedings of the IASTED International Conference on Robotics and Applications*, ISBN: 0-88986-313-x, Tampa, FL (Nov. 2001) pp. 101–105.
17. H. Karbasi, Jan P. Huissoon and A. Khajepour, "Uni-drive modular robots: Theory, design and experiments," *J. Mech. Mach. Theory* **39**, 183–200 (2004).
18. W. J. Chen and M. Xie, "On the Design of a Novel Dexterous Hand," *Ninth International Conference on Advanced Robotics*, Tokyo, Japan, (Oct. 25–27, 1992) pp. 61–65.
19. H. Sira-Ramirez, M. Zribi and S. Ahmad, "Pulse width modulated control of robotic manipulator," *Int. J. Syst. Sci.* **24**(8), 1423–1437 (1993).
20. S. Choi and D.-W. Cho, "Control of wheel slip ratio using sliding mode controller with pulse width modulation," *J. Veh. Syst. Dyn.* **39** 267–284 (1999).
21. S.-S. Han, S.-B. Choi and C.-C. Cheong, "Position control of x-y table mechanism using electro-rheological clutches," *J. Mech. Mach. Theory* **35**, 1563–1577 (2000).
22. Hamidreza Karbasi Uni-Drive Modular Robots *Ph.D. Thesis* (Waterloo, Canada: University of Waterloo, 2003).
23. S. J. Park, The Conceptual Design of a Multi-Linked Modular Robot and the Feasibility Study of the Modular Robot Joint Drive Method *Master Thesis* (Waterloo, Canada: University of Waterloo, 2002).
24. K. K. D. Young, "Controller design for a manipulator using theory of variable structure systems," *IEEE Trans. Sys., Man, Cyber.* **SMC-8**(2), 101–109 (Feb. 1978).
25. J. J. E. Slotine and W. Li, *Applied Nonlinear Control* (Prentice Hall, Englewood Cliffs, N.J., 1991).
26. V. I. Utkin, "Variable structure systems with Sliding mode," *IEEE Trans. Autom. Control* **AC-22**(2), 212–222 (Feb. 1977).

https://doi.org/10.1017/S0263574709005670 Published online by Cambridge University Press